JOURNAL OF THERMOPHYSICS AND HEAT TRANSFER
Vol. 11, No. 3, July–September 1997

Nonequilibrium and Differential Diffusion Effects in Turbulent Hydrogen Diffusion Flames

J. P. H. Sanders* and I. Gökalp†
Centre National de la Recherche Scientifique, Orléans 45071, France

The prediction of thermal NO formation in turbulent hydrogen–air diffusion flames is studied using the laminar flamelet concept. Each of the laminar flamelets is subject to a different state of nonequilibrium. The theoretical parameter for this effect is the scalar dissipation rate. In the literature, this parameter sometimes has been interpreted as the strain rate. Recent results imply that only by using the scalar dissipation rate can the experimentally established scaling behavior of the NO emission index be predicted. Detailed comparisons between flamelet-based predictions and measurements of temperature, major species, and NO for diluted turbulent hydrogen diffusion flames are presented. These comparisons show that differential diffusion effects in the laminar flamelets are very important and lead to overpredictions of NO in the far field of turbulent hydrogen flames. Suppressing differential diffusion by assuming unity Lewis numbers for all species is shown to reduce the far-field overpredictions, but it leads to an underestimation of the near-field NO mass fractions. Velocity and scalar (including temperature and NO mass fractions) predictions agree relatively well in the near field of the investigated diluted hydrogen flames.

Nomenclature

a = strain rate
C_p = mixture heat capacity
D = nozzle diameter
$\mathcal{D}$ = diffusion coefficient
$EI\mathrm{NO}_x$ = emission index
F = mean mixture fraction
f = mixture fraction
f''^2 = mean scalar variance
Le = Lewis number
$P(\phi)$ = probability density function of ϕ
r = radial distance
T = temperature
U = mean axial velocity
$\boldsymbol{u}$ = velocity
$\dot{w}_{\mathrm{NO}}$ = production rate of NO
x = axial distance
Y_i = mass fraction of species i
y = spatial normal coordinate in the laminar flamelets
ε_f = mean scalar dissipation rate
λ = mixture heat conductivity
ρ = density
ϕ = generalized variable
χ = instantaneous scalar dissipation rate

Subscripts
j = jet fluid
st = stoichiometric

Superscripts
q = quenching value
$\tilde{\phi}$ = Favre average of ϕ
$\bar{\phi}$ = conventional average of ϕ
$'$ = conventional fluctuation
$''$ = Favre fluctuation

Presented as Paper 96-3033 at the AIAA/ASME/SAE/ASEE 32nd Joint Propulsion Conference, Lake Buena Vista, FL, July 1–3, 1996; received Aug. 12, 1996; revision received Jan. 27, 1997; accepted for publication Jan. 27, 1997.

*Postdoctoral Researcher, Laboratoire de Combustion et Systèmes Réactifs. E-mail: sanders@cnrs-orleans.fr. Member AIAA.

†Senior Scientist, Laboratoire de Combustion et Systèmes Réactifs. Member AIAA.

I. Introduction

NO production is important in the context of current increasing regulations on pollutant emissions on, for instance, aircraft engines. Turbulent hydrogen jet diffusion flames represent a useful test case for turbulent combustion models because they combine a relative simplicity of the flowfield, well-known chemical kinetics, and challenging turbulence–chemistry interactions such as nonequilibrium effects and differential diffusion effects. Turns[1] recently reviewed the experimental and modeling efforts in this field. One of the current turbulent combustion models that includes nonequilibrium and differential diffusion effects is the laminar flamelet model for turbulent combustion.[2] This model is based on a conserved scalar (mixture fraction) approach and nonequilibrium effects are taken into account by the local scalar dissipation rate. The model views the turbulent flame as an ensemble of laminar one-dimensional stretched diffusion flamelets. These laminar flames are computed including detailed chemistry. When detailed molecular transport is used, differential diffusion effects are present. An important aspect of the flamelet method is its ability to take nonequilibrium effects into account. These nonequilibrium effects provoke a reduction in flame temperature and changes in radical species concentrations. This can strongly influence pollutant formation, such as NO production.

Of particular interest is the global scaling behavior of the NO emission index $EI\mathrm{NO}_x$ as a function of the burner exit parameters such as U_j, D, and the fuel dilution. The $EI\mathrm{NO}_x$ is defined as the total mass (g) of NO produced per kg of fuel injected. Experimental data in Refs. 3 and 4 showed a scaling with a slope 0.5 on a log–log plot of $EI\mathrm{NO}_x$ vs the global flame Damköhler number. These data have been used to test turbulent combustion models. In particular, the joint probability density function (PDF) transport equation method,[5] applied in Refs. 6 and 7, reproduces this scaling behavior. The conditional moment closure (CMC) method[8] also produces approximately a 0.5 slope. However, chemical equilibrium models[9–12] give a slope of 1, which clearly indicates that

nonequilibrium effects are important and equilibrium models cannot be used for NO predictions.

The flamelet model needs a parameter that quantifies nonequilibrium effects. Theoretically this is the scalar dissipation rate, as mentioned earlier, but often the strain rate has been used instead.[13–17] Sanders and Gökalp[18] showed semianalytically that using the strain rate will give a slope even larger than 1, which means that nonequilibrium effects quantified by the strain rate work in the wrong direction. Performing full turbulent flame calculations, Sanders et al.[19] recently showed that the correct 0.5 slope is obtained with the flamelet method, when the scalar dissipation rate is used as the nonequilibrium parameter. However, absolute values of $EINO_x$ are a factor of 10 too high and this is attributed to differential diffusion effects. Preferential diffusion of H_2 with respect to other species leads to a relative increase of H_2 molecules that reach the flame zone, and thus to an increase of the flame temperature with respect to the case where all diffusivities are equal. These high flame temperatures also lead to high NO production rates.

In the present study, the characteristics of the flamelet model are investigated in more detail by making detailed comparisons with the experimental data of Meier et al.[20] on diluted H_2–N_2 turbulent diffusion flames, which include data on NO mass fractions.

II. Turbulent Combustion Model

A second-order turbulence model based on the work of Launder et al.[21] is used, but with a different constant for the return to isotropy term to account for the problem of predicting accurately the spreading rates of round jets. Buoyancy effects in the mean axial momentum equation and buoyancy-induced turbulence production are taken into account as well. The model is given in detail in Ref. 22 as the model RSM II. The same model, but without buoyancy terms, has also been given in Ref. 19.

In the present flamelet method, the instantaneous thermochemical state of the flame depends on the combustion invariant f and on a nonequilibrium parameter. In line with our previous study,[19] the nonequilibrium parameter is assigned as χ, i.e., $\phi = \phi(f, \chi)$. The scalar dissipation rate is defined as

$$\chi = 2\mathcal{D}\frac{\partial f''}{\partial x_j}\frac{\partial f''}{\partial x_j}$$

where $\mathcal{D}$ is a representative molecular diffusion coefficient. The mixture fraction in the laminar flamelets is taken to be the hydrogen element mass fraction.

The (Favre) mean of a thermochemical variable that obeys fast chemical kinetic processes is obtained by averaging the laminar flamelet data over the mixture fraction and the scalar dissipation rate. Thus, the mean of a variable ϕ, which can be T, Y_i, or $\bar{\dot{w}}_{NO}$ (but not $\tilde{Y}_{NO}$, see the following text), is then

$$\tilde{\phi} = \int_0^1 \mathrm{d}f \int_0^\infty \mathrm{d}\chi \tilde{P}(f, \chi)\phi(f, \chi)$$
$$(\bar{\rho})^{-1} = \int_0^1 \mathrm{d}f \int_0^\infty \mathrm{d}\chi \frac{\tilde{P}(f, \chi)}{\rho(f, \chi)} \quad (1)$$

Here, $\tilde{P}(f, \chi)$ is the joint PDF of f and χ. The variables $\phi(f, \chi)$ are a function of the mixture fraction at a given value of χ. In general, the scalar dissipation rate at stoichiometric mixture χ_{st} is used. One possibility to calculate $\phi(f, \chi_{st})$ is to solve the system of differential equations in a quasi-one-dimensional diffusion flame in the counterflow configuration. Such a flame is subjected to flame stretch, quantified by χ_{st} and the thermochemical quantities are a function of f only. About 20 planar flamelets are used at different values of the scalar dissipation rate $\chi_{i,st}$ with $i = 1 \ldots n_f$, where n_f is the number of flamelets for a given dilution. Formally, the method of using Eq. (1) is adequate for quantities that are a function of f and χ_{st} only, which restricts the procedure to fast, diffusion-limited, chemical processes. The slow, kinetically-limited, production of NO must therefore be obtained by solving the transport equation for $\tilde{Y}_{NO}$

$$\nabla\cdot(\bar{\rho}\tilde{\boldsymbol{u}}\tilde{Y}_{NO}) = -\nabla\cdot\widetilde{\boldsymbol{u}''Y''_{NO}} + \bar{\dot{w}}_{NO} \quad (2)$$

The mean rate $\bar{\dot{w}}_{NO}$ in Eq. (2) is obtained by weighting the instantaneous rate $\dot{w}_{NO}$ according to Eq. (1).

The joint PDF $P(f, \chi_{st})$ is modeled as $P(f)P(\chi_{st})$. $P(f)$ is approximated by a β function using the first two moments, namely, $\tilde{f}$ and $\widetilde{f''^2}$, which can both be obtained by classically modeled transport equations (see also Refs. 16 and 23). The scalar dissipation rate model is based on proportionality of mechanical and scalar time scales. Its PDF is modeled either as a lognormal distribution or as a delta fuction at the mean value, thus neglecting turbulent fluctuations. In the present study the delta function is used.

Local flame extinction is not considered in these flames, which means that if the local turbulent value of χ_{st} exceeds the maximum value of $\chi_{i,st}$, the flamelet with the maximum value of χ_{st} is taken. The neglect of local extinction is not considered a limitation because the largest contribution to the total NO production comes from the downstream flame regions where no local extinction effects are expected.

III. Laminar Flamelet Calculations

The laminar flamelet calculations are performed with a code developed by Rogg.[24] For a description of the equations that are solved, for references for the numerical methods, and for the hydrogen combustion mechanism used, see Ref. 25. For each flamelet the strain rate at the oxidizer side a is imposed, and values for a are chosen between 1 s^{-1} and the extinction value a_q. To describe nonequilibrium effects, the flamelet method needs the scalar dissipation rate at stoichiometric conditions χ_{st}, as described earlier. This value is evaluated from the calculated mixture fraction profile as

$$\chi = 2\mathcal{D}\frac{\partial f}{\partial y}\frac{\partial f}{\partial y}$$

There exists an approximate proportionality in laminar flamelets between a and χ_{st}. However, this proportionality does not hold for the mean values of these parameters in turbulent jet flames.

The formation of thermal NO is described by the extended Zeldovich mechanism (see Table 1). Since the reaction $N_2 + O \leftrightarrows NO + N$ is the slowest, and thus rate determining, this single reaction can be taken as an approximation of the whole NO system. The thermochemical quantities of primary importance for NO formation are the temperature and the oxygen radical concentration. The chemical kinetic scheme is given in Table 1.

As mentioned in Sec. I, differential diffusion effects are important in hydrogen diffusion flames. This can be illustrated by comparing flamelet computations, which include differential diffusion effects as a result of use of detailed molecular transport models, to equilibrium values. In Fig. 1 the flamelet temperatures are shown as a function of the H-element-based mixture fraction for various strain rates between a = 1/s and 10,000/s. The extinction strain rate is a_q = 11,650/s, which is lower than the one for pure H_2–air flamelets (a_q = 14,000/s). Figure 1 shows that the temperature strongly decreases with increasing strain rate. The chemical equilibrium temperature is also plotted. If all diffusivities in the flamelets had been equal, all of the flamelet temperatures would be lower than the equilibrium temperature. However, Fig. 1 shows higher maximum flamelet temperatures at stoichiometry for all strain rates $a <$

Table 1 Hydrogen reaction mechanism, including the thermal NO scheme[a]

Number	Reaction	B	α	E
1	$H + O_2 \rightarrow OH + O$	2.000×10^{14}	0.00	70.300
2	$OH + O \rightarrow H + O_2$	1.568×10^{13}	0.00	3.520
3	$H_2 + O \rightarrow OH + H$	5.060×10^{4}	2.67	26.300
4	$OH + H \rightarrow H_2 + O$	2.222×10^{4}	2.67	18.290
5	$H_2 + OH \rightarrow H_2O + H$	1.000×10^{8}	1.60	13.080
6	$H_2O + H \rightarrow H_2 + OH$	4.312×10^{8}	1.60	76.460
7	$OH + OH \rightarrow H_2O + O$	1.500×10^{9}	1.14	0.420
8	$H_2O + O \rightarrow OH + OH$	1.473×10^{10}	1.14	71.090
9	$H + O_2 + M' \rightarrow HO_2 + M'$	2.300×10^{18}	−0.80	0.000
10	$HO_2 + M' \rightarrow H + O_2 + M'$	3.190×10^{18}	−0.80	195.390
11	$HO_2 + H \rightarrow OH + OH$	1.500×10^{14}	0.00	4.200
12	$HO_2 + H \rightarrow H_2 + O_2$	2.500×10^{13}	0.00	2.900
13	$HO_2 + OH \rightarrow H_2O + O_2$	6.000×10^{13}	0.00	0.000
14	$HO_2 + H \rightarrow H_2O + O$	3.000×10^{13}	0.00	7.200
15	$HO_2 + O \rightarrow OH + O_2$	1.800×10^{13}	0.00	−1.700
16	$HO_2 + HO_2 \rightarrow H_2O_2 + O_2$	2.500×10^{11}	0.00	−5.200
17	$OH + OH + M' \rightarrow H_2O_2 + M'$	3.250×10^{22}	−2.00	0.000
18	$H_2O_2 + M' \rightarrow OH + OH + M'$	1.692×10^{24}	−2.00	202.29
19	$H_2O_2 + H \rightarrow H_2O + OH$	1.000×10^{13}	0.00	15.000
20	$H_2O_2 + OH \rightarrow H_2O + HO_2$	5.400×10^{12}	0.00	4.200
21	$H_2O + HO_2 \rightarrow H_2O_2 + OH$	1.802×10^{13}	0.00	134.750
22	$H + H + M' \rightarrow H_2 + M'$	1.800×10^{18}	−1.00	0.000
23	$OH + H + M' \rightarrow H_2O + M'$	2.200×10^{22}	−2.00	0.000
24	$O + O + M' \rightarrow O_2 + M'$	2.900×10^{17}	−1.00	0.000
25	$N_2 + O \rightarrow NO + N$	1.900×10^{14}	0.00	319.030
26	$NO + N \rightarrow N_2 + O$	4.22047×10^{13}	0.00	4.253
27	$NO + H \rightarrow N + OH$	1.300×10^{14}	0.00	205.850
28	$N + OH \rightarrow NO + H$	4.80384×10^{13}	0.00	5.270
29	$NO + O \rightarrow N + O_2$	2.400×10^{9}	1.00	161.670
30	$N + O_2 \rightarrow NO + O$	1.13052×10^{10}	1.00	27.838

[a]Most of the data are taken from Ref. 25. The reaction rate k_k of the kth reaction is given by $k_k = B_k T_k^{\alpha} \exp(-E_k/R_u T)$, with the activation energy E_k in kJ/mole and R_u is the universal gas constant. Third body coefficients are H_2O, 6.5; O_2, 0.4; and N_2, 0.4.

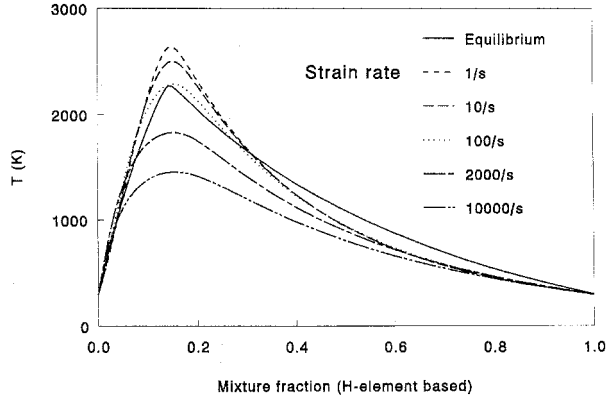

Fig. 1 Flamelet temperatures at various strain rates and the equilibrium temperature for the 75% H_2–25% N_2 flamelets.

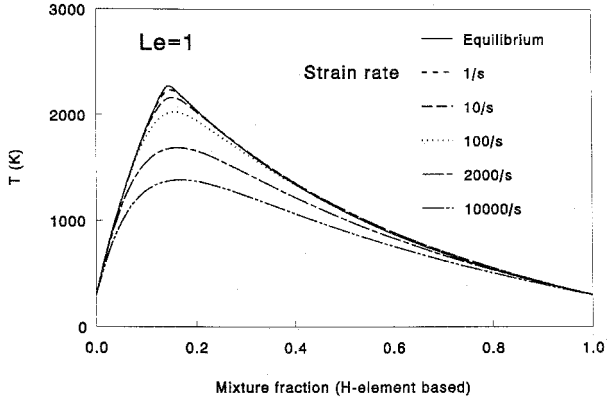

Fig. 2 Flamelet temperatures for $Le_i = 1$ at various strain rates and the equilibrium temperature for the 75% H_2–25% N_2 flamelets.

100/s. This is because of the previously mentioned differential diffusion effects. Only for higher strain rates does the maximum flamelet temperature decrease below the equilibrium value. To show the effect of equal diffusivities for all species, the diffusion fluxes in the flamelet calculation are evaluated by setting the Lewis number for all species equal to one, i.e., $Le_i = \lambda/\rho C_p \mathcal{D} = 1$. The conductivity λ has been set to its value for N_2. In Fig. 2 the resulting flamelet temperatures are shown, again together with the equilibrium values. Indeed, all flamelet temperatures are below equilibrium, as expected, and weakly strained flamelets approach the equilibrium values.

Nonequilibrium effects on the NO production rate as a function of the mixture fraction for various strain rates are shown in Fig. 3. The increasing maximum production rate with strain rate, which was shown in Ref. 19 to be very important regarding $EINO_x$ scaling behavior, can be observed. Also, the production rate at low strain rates is negative in the fuel-rich zone, and this effect diminishes for higher strain rates. The equilibrium values are much smaller than those for flamelets at low strain. This again is because of the superequilibrium flamelet temperatures at low strain rates. The effect is of particular importance for the prediction of NO formation in the far field of a turbulent jet flame where strain rates are low. In Fig. 4 the flamelet NO production rates with $Le_i = 1$ are still higher than the equilibrium value, but the maximum difference now is about a factor 2, whereas it is more than a factor 10 for the flamelets with full differential transport. Moreover, the flamelet peak values occur at the same value of the mixture fraction as the equilibrium peak value.

IV. Predictions of Turbulent Diffusion Flames

The vertical diluted hydrogen flames (75% H_2/25% N_2), measured at DLR Stuttgart,[20] are now considered. The nozzle diameter is $D = 0.008$ m, and exit velocities are $U_j =$

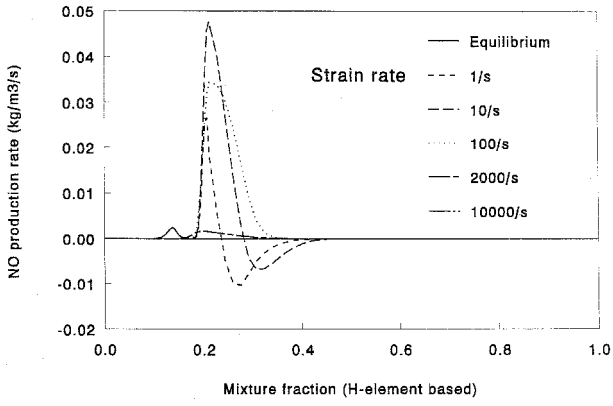

Fig. 3 Flamelet NO production rates [kg/(m^3 s)] at various strain rates and the equilibrium values for the 75% H_2–25% N_2 flamelets.

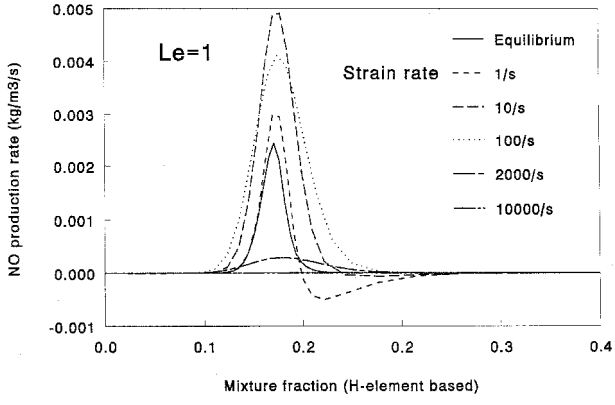

Fig. 4 Unity Lewis number flamelet NO production rates [kg/(m^3 s)] at various strain rates and the equilibrium values for the 75% H_2–25% N_2 flamelets.

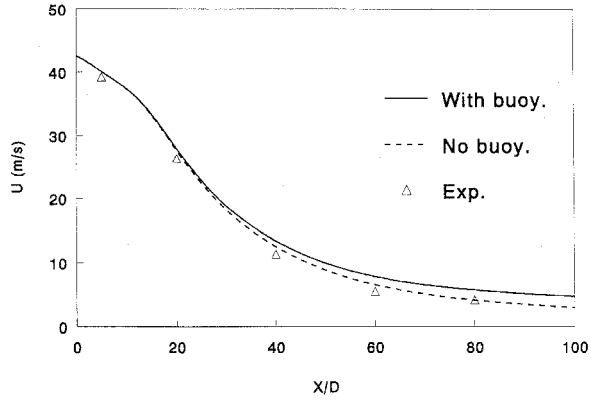

Fig. 5 Centerline variation of the mean axial velocity for the flame measured at TH Darmstadt. Solid line: predictions including buoyancy effects. Dashed line: predictions without buoyancy effects. Symbols represent measurements of Ref. 26.

56.4, 42.3, 28.2, and 14.1 m/s, with a coflow of U_{coflow} = 0.3 m/s. The Reynolds and Froude numbers of these flames are (Re, Fr) = (1.42 × 10^4, 40,530); (1.0650 × 10^4, 22,800); (7.1 × 10^3, 10,130); and (3.35 × 10^3, 2530), respectively. The Reynolds number of the latter flame (14.1 m/s, 3.35 × 10^3) is too low and it is not computed.

The DLR measured scalar quantities, whereas velocity measurements for a similar flame on the same type of burner (50% H_2/50% N_2 at U_j = 34.8 m/s) were performed at the Technische Hochschule (TH) Darmstadt.[26] The axial centerline mean velocity for this flame is predicted relatively well as can be seen in Fig. 5. However, the predictions without buoyancy agree better in the far field than those including buoyancy effects. Since it will be shown that flamelet-based temperatures and NO mass fractions are most accurately predicted in the near field because of differential diffusion issues, we will concentrate most on the near field. All of the following predictions include gravity effects. Radial profiles of the axial velocity from x/D = 5 to 40 are given in Fig. 6. The experiments and computations agree very well. Although the fuel of the Darmstadt flame is a little more diluted, it can be expected that also the velocity fields of the Stuttgart flame are well predicted.

The mean centerline mixture fraction, based on the hydrogen element mass fractions shown in Fig. 7, is well predicted. The centerline scalar fluctuation intensities

$$\sqrt{\widetilde{f''^2}}/F$$

are shown in Fig. 8. Both predictions and measurements show an increase of the fluctuation level with decreasing exit velocity. This is because of gravity effects that become more important at lower velocities. When gravity effects are present, F decays more rapidly with x (Ref. 22), which explains the higher values of

$$\sqrt{\widetilde{f''^2}}/F$$

This can be observed in Fig. 8, in which a computation without gravity for the U_j = 42.3 m/s flame is given as a dotted line. Centerline mean temperatures predicted with the flamelet method with Le = 1 are shown in Fig. 9. The far-field temperature levels are lower for the flames at lower exit velocities

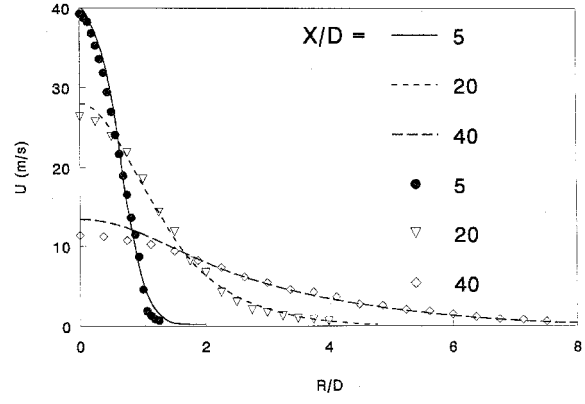

Fig. 6 Axial velocity across the flame measured at TH Darmstadt[26] at various axial stations. Lines are predictions and symbols represent measurements.

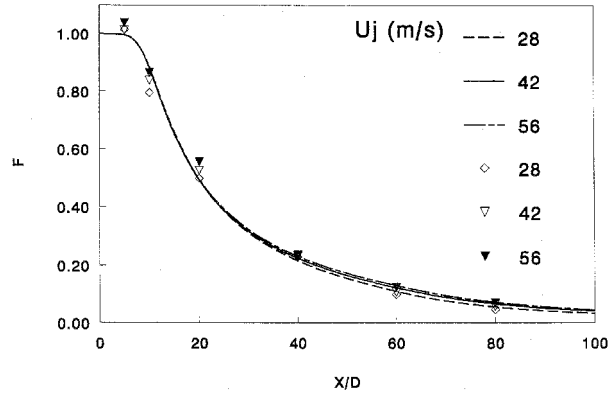

Fig. 7 Centerline variation of the mixture fraction for three flames measured at DLR Stuttgart.[20] Lines are predictions and symbols represent measurements.

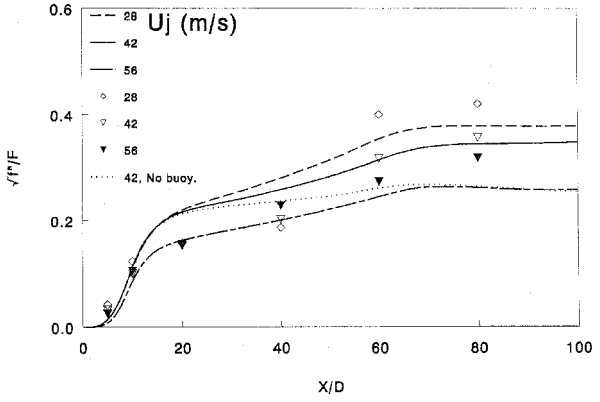

Fig. 8 Centerline variation of the mixture fraction fluctuation intensity $\sqrt{f''^2}/F$ for three flames measured at DLR Stuttgart.[20] See Fig. 7 for details. The dotted line represents the 42.3 m/s flame without buoyancy effects.

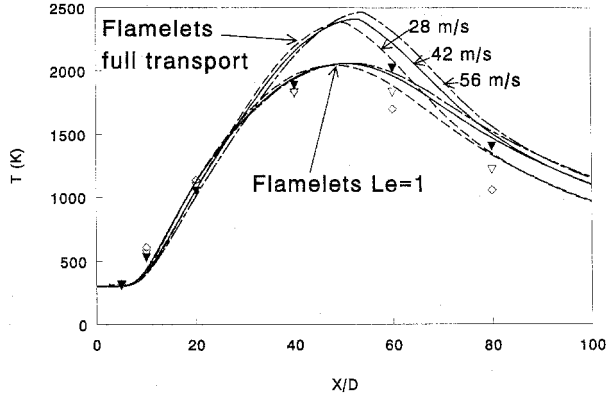

Fig. 9 Centerline temperature variation predicted with the flamelet model for three flames measured at DLR Stuttgart.[20] The upper curves correspond to the flamelet model including differential diffusion effects and the lower curves to the flamelet model with $Le = 1$. See Fig. 7 for details.

because of the faster mixture fraction decay and the higher scalar fluctuation intensities at lower exit velocities. The scalar fluctuation intensity leads to the effect of unmixedness, which can be quantified as $\widetilde{f''^2}/\tilde{F}(1 - \tilde{F})$, and which also reflects the intensity of turbulent scalar fluctuations. If, for instance, the unmixedness is large while the mean mixture fraction is stoichiometric, the mean flame temperature will be lower than its stoichiometric value because the fuel and oxidizer do not coexist at the same time at the same location. Exactly the same effect can be observed when the flamelet method including differential diffusion is used to compute the thermochemical state (Fig. 9). However, the mean temperatures near the flame tip are now higher than with the $Le = 1$ assumption because of the differential diffusion effects. The $Le = 1$ values are closer to the experimental data because, as shown by Meier et al.,[20] differential diffusion effects in turbulent jet flames are mainly important close to the nozzle. In both the near and far field, the centerline temperature is predicted well by both flamelet models, including and excluding differential diffusion. This is because in these fuel-rich and fuel-lean regions, strain rate variations are not very influential, since strain-induced temperature variations are limited to mixture fraction values around stoichiometry.

Figure 10 shows centerline major species mole fractions for the 42.3-m/s flame. The flamelet and equilibrium predictions do not differ very much and both agree relatively well with the experiments, because the major species are not so much affected by nonequilibrium chemistry effects.

The centerline NO mass fraction predictions are shown in Fig. 11. The experimental maximum values are about two times higher than the $Le = 1$ results. The full transport flamelet results are much higher than the experimental data, which was to be expected in view of the overpredicted absolute $EINO_x$ values.[19] However, the variation of the predicted levels with the exit velocity is predicted relatively well, which again indicates that nonequilibrium effects are taken into account correctly.

Now, radial profiles at $x/D = 5$ are considered. Figure 12 shows that the H-element-based mixture fraction across the jet is predicted very well. It appears that differential diffusion, which is most important at low exit velocities and close to the nozzle,[20] leads to slightly higher values of the H-element mass

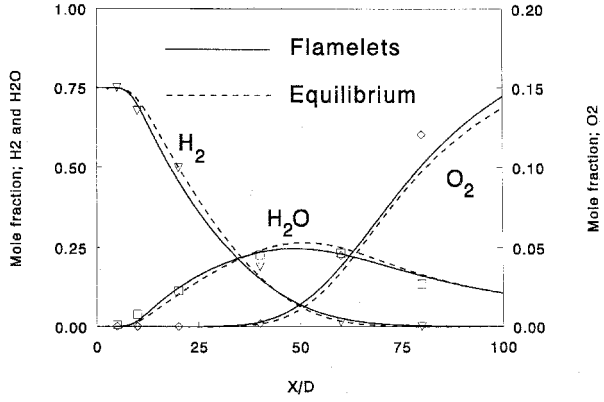

Fig. 10 Centerline composition for the 42.3 m/s flame, predicted with equilibrium chemistry and flamelets. Experiments of DLR Stuttgart.[20] See Fig. 7 for details.

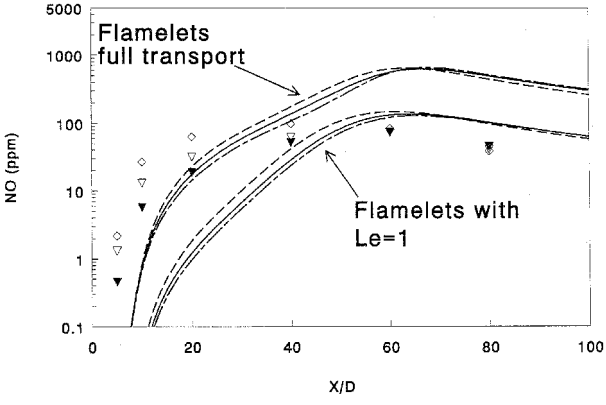

Fig. 11 Centerline variation of the NO mole fraction in ppm predicted with the flamelet model. Upper curves correspond to the flamelet model with differential diffusion effects, lower curves to flamelet results with $Le = 1$. Experiments of DLR Stuttgart.[20] See Fig. 7 for details.

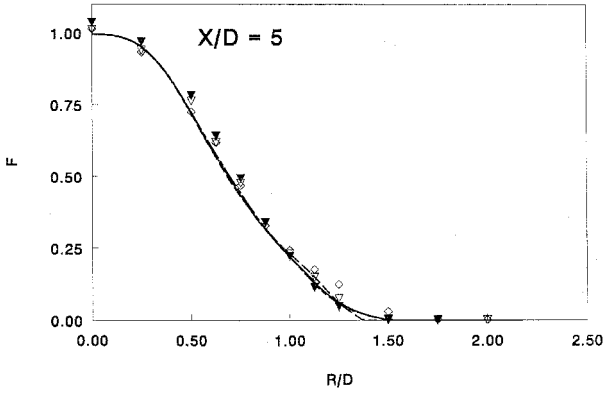

Fig. 12 Radial mixture fraction profiles at $X/D = 5$. See legend of Fig. 7 for details.

fraction at the air side of the mixing layer. The mean mixture fraction equation does not account for this effect because differential diffusion is not taken into account. The scalar variance across the jet at the same axial station (Fig. 13) is somewhat overpredicted near the air side of the mixing layer. This overprediction will influence the temperature predictions in this region. The temperature profiles at this axial station (Fig. 14) agree relatively well with the experiments, except for the height of the peak, which is underpredicted with both models, possibly because of the overpredicted scalar variance. There is only a small difference between the models because near stoichiometry the strain rate is such that the flamelet and equilibrium temperature are very close. The low values of the predicted temperatures can be the result of either an overpredicted strain rate or an overpredicted variance of the mixture fraction. Analyzing the numerical values of $\tilde{a}$ and $\widetilde{f''^2}$ at $F \approx f_{st}$ shows that with the local value of $\widetilde{f''^2} = 0.013$, the mean experimental temperature of $T_{max} \approx 2241$ K cannot be reproduced, not even with the lowest strain rate in the flamelet library of $a = 1\ s^{-1}$. This implies that close to the nozzle the mixture fraction fluctuations are overpredicted, which was already shown in Fig. 13. The radial profiles of the mole fractions at $x/D = 5$ are shown in Fig. 15. The agreement between experiments and predictions is very satisfactory for both models. Figure 16 shows that the flamelet NO levels including differential diffusion are closest to the experimental values (within a factor 2). Equilibrium chemistry underpredicts the NO level by a factor of almost 70. The $Le = 1$ flamelet results show even lower levels because of nonequilibrium effects. This indicates the importance of differential diffusion effects in the near field. Turbulent fluctuations of the scalar dissipation rate have a negligible influence, as can be seen from the curve labeled lognormal, indicating the use of a lognormal PDF for the scalar dissipation rate with variance 1. The experimental NO level rises earlier than the predictions, while going from rich to lean

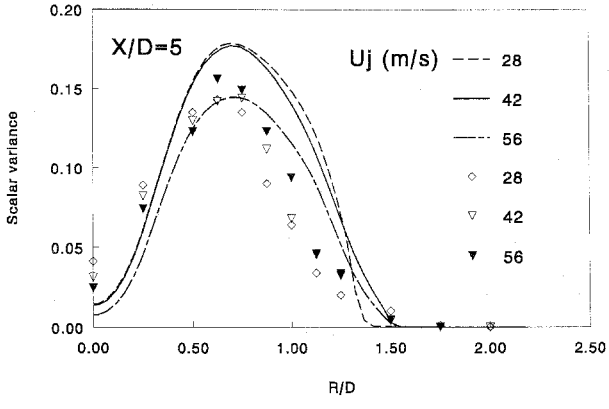

Fig. 13 Radial scalar variance profiles at $X/D = 5$. See legend of Fig. 7 for details.

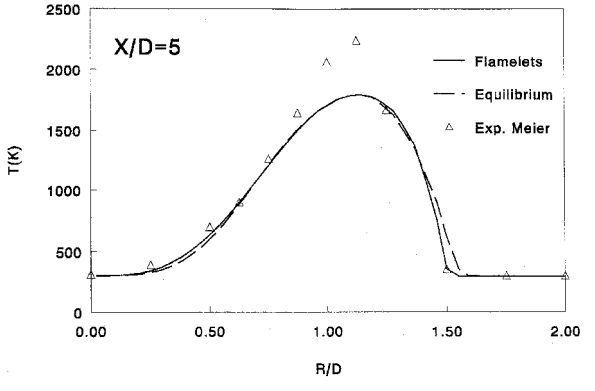

Fig. 14 Radial temperature profiles at $X/D = 5$. See legend of Fig. 7 for details.

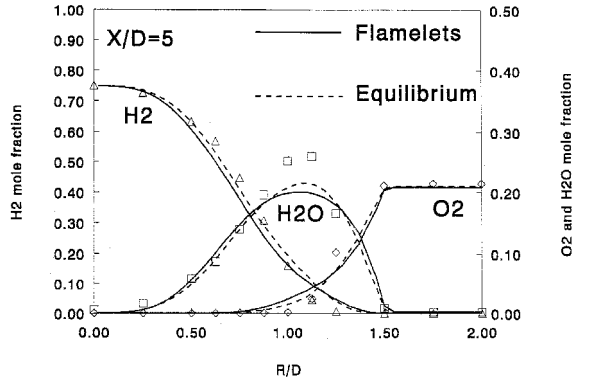

Fig. 15 Radial profiles of stable species at $X/D = 5$. See legend of Fig. 7 for details.

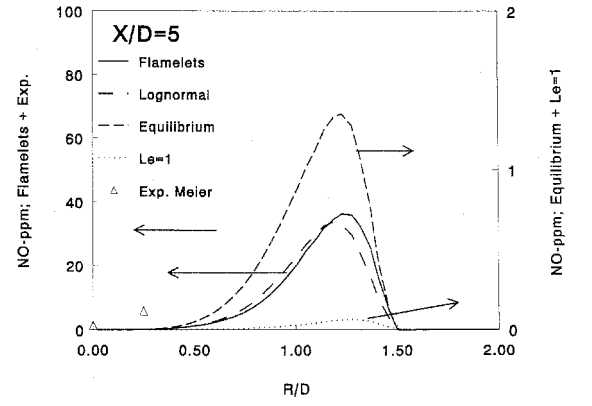

Fig. 16 Radial profiles of the NO mole fraction in ppm at $X/D = 5$. The solid line represents the flamelet results with differential diffusion but without scalar dissipation rate fluctuations (delta function PDF). The long-dashed curve shows the effect of including a lognormal distribution for the scalar dissipation rate with variance 1. The dashed line is the equilibrium chemistry curve and the dotted line the $Le = 1$ flamelet result. Symbols are the experimental data of Meier et al.[20] Note the scale difference on the left and right vertical axes.

mixtures. This was also observed with the centerline variation of the NO level and still awaits an explanation.

V. Conclusions

Detailed comparisons of predictions and measurements of diluted turbulent hydrogen flames have been presented. Computations of the velocity and mixture fraction field, obtained with a second-order turbulence model, agree well with the measurements of Darmstadt[26] and Stuttgart.[20] Predictions of the mean thermochemical variables were made with the laminar flamelet method. They show that flamelet-based temperatures and NO mass fractions in the far field are overpredicted because of the differential diffusion effects in the laminar flamelets. Major species are less influenced by these effects. However, in the near field differential diffusion effects are present in the turbulent flames and the effects should be included in the flamelets. Reducing the effect of differential diffusion in the flamelets by assuming unity Le numbers for all species improves the far-field predictions significantly, but NO mass fractions are then strongly underpredicted in the near field. The trend of the nonequilibrium effects on the NO mass fractions for jet flames at different exit velocities is well reproduced with the flamelet method. In general, the near-field predictions can be concluded to be satisfactory with the current model; however, modifications of the flamelet model, notably regarding differential diffusion effects, are necessary in the far field. These modifications will be less important when other

fuels, such as hydrocarbons, are considered, where differences between the diffusion coefficients are less important.

Future work on flamelet predictions will include radiation effects that can play a role regarding NO production. Also, the suppression of differential diffusion effects should depend on a criterion such that differential diffusion is present in the near field, and is suppressed in the far field. Globally, differential diffusion effects should diminish with the turbulent Reynolds number.

Acknowledgments

The French Ministry of Foreign Affairs is gratefully acknowledged for the postdoctoral fellowship of J. P. H. Sanders. We also thank V. Bergmann and W. Meier of DLR, Stuttgart, Institute of Physical Chemistry for kindly providing their experimental scalar data. E. Hassel from the Technische Hochschule, Darmstadt is thanked for sending the velocity data.

References

[1]Turns, S. R., "Understanding of NO_x Formation in Nonpremixed Flames: Experiments and Modeling," *Progress in Energy and Combustion Science*, Vol. 21, No. 5, 1995, pp. 361–386.

[2]Peters, N., "Laminar Flamelet Concepts in Turbulent Combustion," *21st Symposium (International) on Combustion*, The Combustion Inst., Pittsburgh, PA, 1986, pp. 1231–1250.

[3]Chen, R.-H., and Driscoll, J. F., "Nitric Oxide Levels of Jet Diffusion Flames: Effects of Coaxial Air and Other Mixing Parameters," *23rd Symposium (International) on Combustion*, The Combustion Inst., Pittsburgh, PA, 1990, pp. 281–288.

[4]Driscoll, J. F., Chen, R.-H., and Yoon, Y., "Nitric Oxide Levels of Turbulent Jet Diffusion Flames: Effects of Residence Time and Damkohler Number," *Combustion and Flame*, Vol. 88, 1992, pp. 37–49.

[5]Pope, S. B., "Pdf Methods for Turbulent Reactive Flows," *Progress in Energy and Combustion Science*, Vol. 11, 1985, pp. 119–192.

[6]Chen, J.-Y., and Kollmann, W., "PDF Modeling and Analysis of Thermal NO Formation in Turbulent Nonpremixed Hydrogen-Air Jet Flames," *Combustion and Flame*, Vol. 88, 1992, pp. 397–412.

[7]Chen, J.-Y., Chang, W.-C., and Koszykowski, M., "Numerical Simulation and Scaling of NO_x Emissions from Turbulent Hydrogen Jet Flames with Various Amounts of Helium Dilution," *Combustion Science and Technology*, Vols. 110 and 111, 1996, pp. 505–529.

[8]Smith, N. S. A., Bilger, R. W., and Chen, J.-Y., "Modelling of Nonpremixed Hydrogen Jet Flames Using a Conditioned Moment Closure Method," *24th Symposium (International) on Combustion*, The Combustion Inst., Pittsburgh, PA, 1992, pp. 263–269.

[9]Peters, N., and Donnerhack, S., "Structure and Similarity of Nitric Oxide Production in Turbulent Diffusion Flames," *18th Symposium (International) on Combustion*, The Combustion Inst., Pittsburgh, PA, 1981, pp. 33–42.

[10]Bilger, R. W., "Reaction Zone Thickness and Formation of Nitric Oxide in Turbulent Diffusion Flames," *Combustion and Flame*, Vol. 26, No. 1, 1976, pp. 115–123.

[11]Peters, N., "An Asymptotic Analysis of Nitric Oxide Formation in Turbulent Diffusion Flames," *Combustion Science and Technology*, Vol. 19, Nos. 1, 2, 1978, pp. 39–49.

[12]Janicka, J., and Peters, N., "Asymptotic Evaluation of the Mean NO-Production Rate in Turbulent Diffusion Flames," *Combustion Science and Technology*, Vol. 22, Nos. 1, 2, 1980, pp. 93–96.

[13]Bray, K. N. C., and Peters, N., *Turbulent Reacting Flows*, edited by P. A. Libby and F. A. Williams, Academic, 1993, pp. 63–113.

[14]Bradley, D., Gaskell, P. H., and Lau, A. K. C., "A Mixedness-Reactedness Flamelet Model for Turbulent Diffusion Flames," *23rd Symposium (International) on Combustion*, The Combustion Inst., Pittsburgh, PA, 1990, pp. 685–692.

[15]Fairweather, M., Jones, W. P., Lindstedt, R. P., and Marquis, A. J., "Predictions of a Turbulent Reacting Jet in a Crossflow," *Combustion and Flame*, Vol. 84, 1991, pp. 361–375.

[16]Sanders, J. P. H., and Lamers, A. P. G. G., "Modeling and Calculation of Turbulent Lifted Diffusion Flames," *Combustion and Flame*, Vol. 96, 1994, pp. 22–33.

[17]Müller, C. M., Breitenbach, H., and Peters, N., "Partially Premixed Turbulent Flame Propagation in Jet Flames," *25th Symposium (International) on Combustion*, The Combustion Inst., Pittsburgh, PA, 1994, pp. 1099–1106.

[18]Sanders, J. P. H., and Gökalp, I., "Flamelet Based Predictions and Scaling Laws of NO-Formation in Turbulent Hydrogen Diffusion Flames," *Proceedings of 8th International Symposium on Transport Phenomena in Combustion*, Taylor and Francis, Washington, DC, 1996, pp. 286–297.

[19]Sanders, J. P. H., Chen, J.-Y., and Gökalp, I., "Flamelet Based Modeling of NO Formation in Turbulent Hydrogen Jet Diffusion Flames," *Combustion and Flame* (to be published), 1997.

[20]Meier, W., Vyrodov, A. O., Bergmann, V., and Stricker, W., "Simultaneous Raman/LIF Measurements of Major Species and NO in Turbulent H_2/Air Diffusion Flames," *Applied Physics B*, Vol. 63, 1996, pp. 79–90.

[21]Launder, B. E., Reece, G. J., and Rodi, W., "Progress in the Development of a Reynolds-Stress Turbulence Closure," *Journal of Fluid Mechanics*, Vol. 68, 1975, pp. 537–566.

[22]Sanders, J. P. H., Sarh, B., and Gökalp, I., "Variable Density Effects in Axisymmetric Isothermal Jets: A Comparison Between a First- and a Second-Order Turbulence Model," *International Journal of Heat and Mass Transfer*, Vol. 40, No. 4, 1997, pp. 823–842.

[23]Sanders, J. P. H., and Lamers, A. P. G. G., "Scalar Transport in a Turbulent Jet," *International Communications in Heat and Mass Transfer*, Vol. 19, 1992, pp. 851–858.

[24]Rogg, B., "RUN-1DL: A Computer Program for Simulation of One-Dimensional Chemically Reacting Flows," Cambridge Univ. Rept. CUED/A-THERMO/TR39, 1992.

[25]Peters, N., and Rogg, B. (eds.), *Reduced Kinetic Mechanisms for Applications in Combustion Systems*, Springer–Verlag, Berlin, 1993.

[26]Cheng, T. C., Fruechtel, G., Neuber, A., Lipp, F., Hassel, E., and Janicka, J., "Experimental Data Base for Numerical Simulation of Turbulent Diffusion Flames," *Engineering Research*, Vol. 61, 1995, pp. 165–170.